ACS SENSORS

pubs.acs.org/acssensors

Article

A Dual-Mode NADH Biosensor Based on Gold Nanostars Decorated $CoFe_2$ Metal–Organic Frameworks to Reveal Dynamics of Cell Metabolism

Xiaoping Zhao, Ruoxin Niu, Shu Fan, Xunan Jing, Rui Gao, Hongbo Yang, Heng Wang, Daquan Wang, Zhiwei Yang, Yunchuan Xie, Junjun She, Peng Chen,* and Lingjie Meng*

Cite This: *ACS Sens.* 2022, 7, 2671−2679

Read Online

ACCESS | Metrics & More | Article Recommendations | Supporting Information

ABSTRACT: Nicotinamide adenine dinucleotide (NADH) is central to metabolism and implicated in various diseases. Herein, nanohybrids of gold nanostars and metal−organic frameworks are devised and demonstrated as a dual-mode NADH sensor, for which colorimetric detection is enabled by its peroxidase-like nanozyme property and Raman detection is realized by its surface-enhanced Raman scattering property with the detection limit as low as 28 pM. More importantly, this probe enables real-time SERS monitoring in living cells, providing a unique tool to investigate dynamic cellular processes involving NADH. Our experiments reveal that metabolism dynamics is accelerated by glucose and is much higher in cancerous cells. The SERS results can also be verified by the colorimetric detection. This sensor provides a new potential to detect biomarkers and their dynamics *in situ*.

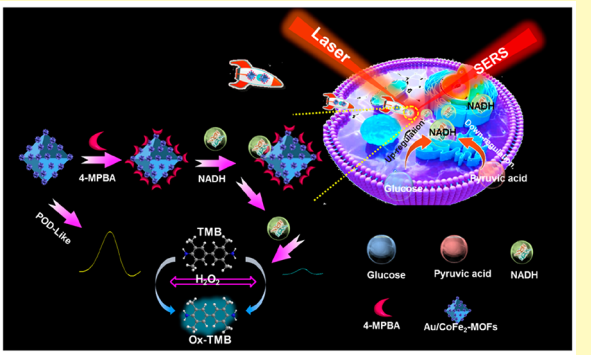

KEYWORDS: *surface-enhanced Raman scattering (SERS), metal−organic frameworks (MOFs), gold nanostars, peroxidase-like, reduced nicotinamide adenine dinucleotide (NADH), cell metabolism*

Nicotinamide adenine dinucleotide (NADH) is an important coenzyme involved in the cytoplasmic glycolysis pathway and respiratory cascade in mitochondria and therefore implicated in various diseases, such as cancer, Alzheimer's disease, and diabetes.[1,2] In living cells, NADH is oxidized to NAD^+ in the electron transport chain of the tricarboxylic acid cycle in glycometabolism, donating its electron for ATP synthesis.[3,4] In addition, NADH is also well-known for its reducing power as a redox cofactor and an up-regulator of the glutathione level.[5] Therefore, endogenous NADH detection is beneficial to revealing its metabolic mechanism and to the diagnosis and treatment of related diseases. Currently, a variety of approaches have been established to detect NADH, such as electrochemical measurement,[6,7] fluorescence detection,[8−10] and high-performance liquid chromatography.[11,12] However, these methods often suffer from many limitations on the *in situ* monitoring of the endogenous NADH in living cells, such as cell destruction, expensive facility, vulnerability to various interferences, slow response, photobleaching, poor reproducibility, or poor specificity.

Surface-enhanced Raman scattering (SERS) spectroscopy is deemed a powerful tool for label-free detection of biomolecules with high specificity and sensitivity.[12−17] More importantly, SERS shows many advantages in preventing photobleaching and autofluorescence, making it a potential technique for quantitative analysis and bioimaging in living cells.[13−15] Generally, noble metal nanostructures (Au, Ag, Cu, etc.) can act as SERS substrates to greatly enhance the Raman signals even over 10 orders of magnitude via electromagnetic enhancement, which are highly suitable for the application of SERS in biomedical applications.[16,17] For example, Masson's group has fabricated SERS nanofibers decorated with plasmonic metal nanoparticles to monitor metabolites under different conditions.[14,15] Specifically, when the SERS nanofiber was modified with a pH-responsive molecule (4-mercaptobenzoic acid), it was able to linearly quantify intracellular pH over the range of 6.5−9.5.[15] Recently, it has been reported that semiconducting metal organic frameworks (MOFs) can magnify Raman signals via chemical enhancement.[18,19] Moreover, MOFs can also act as vehicles to carry individually dispersed SERS-responsive noble nanoparticles.[18] Thus, MOF/noble nanoparticle hybrids can synergistically enhance SERS signals. Besides, MOFs have attracted increasing

Received: June 1, 2022
Accepted: August 15, 2022
Published: August 24, 2022

Scheme 1. Schematic Illustration of a Dual-Mode NADH Biosensor Based on Au/$CoFe_2$-MOFs to Reveal the Dynamics of Cell Metabolism

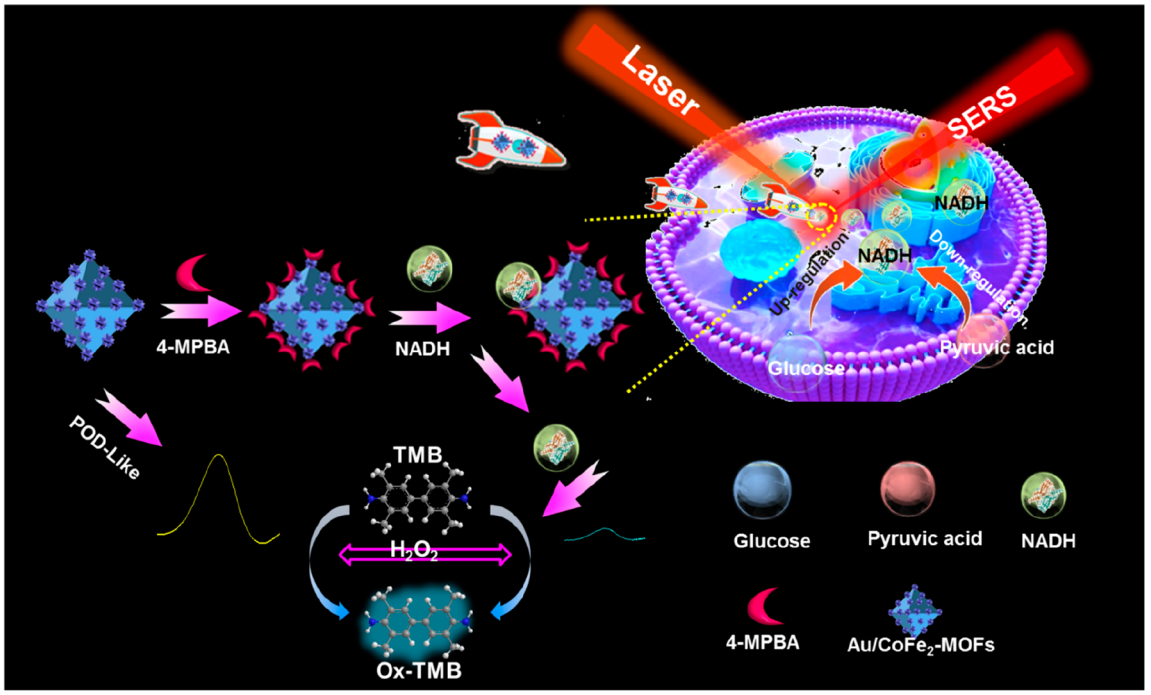

attention in colorimetric detection due to their intrinsic enzyme-like property.[20] Therefore, we conceive that dual-mode sensing systems based on MOF/noble nanoparticles may be designed where colorimetrics can provide convenient ensemble analysis and highly enhanced Raman signals can provide label-free and real-time detection at the cellular level.

Herein, a dual-mode biosensor, gold nanostar/$CoFe_2$-MOF hybrids (Au/$CoFe_2$-MOFs), are devised to detect NADH based on either a colorimetric or SERS mechanism and reveal the dynamics of cell metabolism (Scheme 1). $CoFe_2$-MOF serves not only as a peroxidase-mimicking nanozyme to catalyze the oxidation of 3,3′,5,5′-tetramethylbenzidine (TMB) dye molecules for the colorimetric detection of NADH but also as an enhancer for Raman signal and a carrier of Au nanostars (Au NSs) which present abundant sharp edges and tips to act as SERS-active "hot spots". Such sensors exhibit high sensitivity and specificity toward NADH. Furthermore, it can reveal the intracellular distribution of NADH, its metabolism-dependent dynamics, and the metabolic differences between normal and cancerous cells. The demonstrated strategy may be also applied to other key factors in the intracellular metabolic networks, whereby providing unique tools for both fundamental study of cell biology and diagnosis.

EXPERIMENTAL SECTION

Synthesis of $CoFe_2$-MOFs Hybrids. $FeCl_3{\cdot}6H_2O$ (0.346 mmol, 93.4 mg), $CoCl_2{\cdot}6H_2O$ (0.173 mmol, 41.2 mg), and NH_2−BDC (0.519 mmol, 94.2 mg) are added into the DMF solution (16 mL) to dissolve by sonication for 10 min. Then, the mixture is placed in the microwave reactor at 140 °C for 5 h.[21] The red−black product is collected by centrifugation for 10 min.

Synthesis of the Gold Nanostars (Au NSs). The surfactant-free method is used to prepare Au nanostars. Aqueous $HAuCl_4$ solution (20.0 μL, 10.0 mM) is first mixed with water (1.0 mL), and then $AgNO_3$ solution (3.0 μL, 10.0 mM) is added. After the solutions are thoroughly mixed, fresh ascorbic acid (AA) (4.0 μL, 100 mM) is quickly added and vigorously shaken for 20 s at room temperature. After centrifugation at a speed of 4800 rpm for 10 min, the Au NSs are redispersed in water (1.0 mL) for further use.[22]

Synthesis of Au/$CoFe_2$-MOFs Hybrids. The prepared Au NSs solution (20.0 mL) is used to disperse the synthetic $CoFe_2$-MOFs (20.0 mg) and mixed by sonication for about 60 min. The Au/$CoFe_2$-MOFs are obtained by centrifugation.

NADH Detection by Colorimetric Method. First, NADH solutions with various concentrations (50 μL, 1.93×10^{-1} M to 1.93×10^{-8} M) are incubated with NAc-Ac buffer (pH 4.5, 2800 μL, 20.0 mM). Subsequently, Au/$CoFe_2$-MOFs solution (1.0 mg/mL, 50 μL), H_2O_2 (30 mM, 50 μL), and TMB (30 mM, 50 μL) are added into the above solution. Finally, the absorption spectra of mixed solutions are recorded after being incubated at 25 °C for 2 min.

SERS Measurement. The R6G is used as a Raman probe to estimate the SERS properties of Au/$CoFe_2$-MOFs. In a typical experiment, the Au/$CoFe_2$-MOFs (1.0 mg) are dispersed in 1 mL of R6G solution (10^{-6} M) over the course of 2 h for the SERS measurements. The SERS experiments are performed by Raman spectroscopy (inVia Qontor, Renishaw), and the excitation source is the 785 nm laser. The Enhanced Factor (EF) is calculated by the following equation:[23]

$$\mathrm{EF} = \frac{I_{\mathrm{SERS}}}{I_{\mathrm{ref}}} \times \frac{C_{\mathrm{ref}}}{C_{\mathrm{SERS}}}$$

where I_{SERS} and I_{ref} are the peak intensities of the R6G at 1510 cm^{-1} on the SERS substrate and the reference substrate, respectively. C_{SERS} and C_{ref} are the R6G concentrations on SERS substrates and reference substrates.

NADH Detection by SERS. NADH is examined by Au/$CoFe_2$-MOF substrates. First, the Raman probes are obtained by modifying 4-mercaptophenylboronic acid (MPBA) molecules on the surface of Au/$CoFe_2$-MOFs via Au−S bonds. In brief, the mixture of MPBA (200 μL, 25 mM) in ethanol is added to the Au/$CoFe_2$-MOFs (0.8 mL, 1.0 mg/mL) solution and maintained overnight. After that, the solution is centrifuged at 8000 rpm for 10 min to remove the excess probe. Then, the obtained MPBA-Au/$CoFe_2$-MOFs are dispersed in water or culture medium for the following experiments. Different concentrations of NADH (200 μL) are incubated with MPBA-Au/

https://doi.org/10.1021/acssensors.2c01175
ACS Sens. 2022, 7, 2671−2679

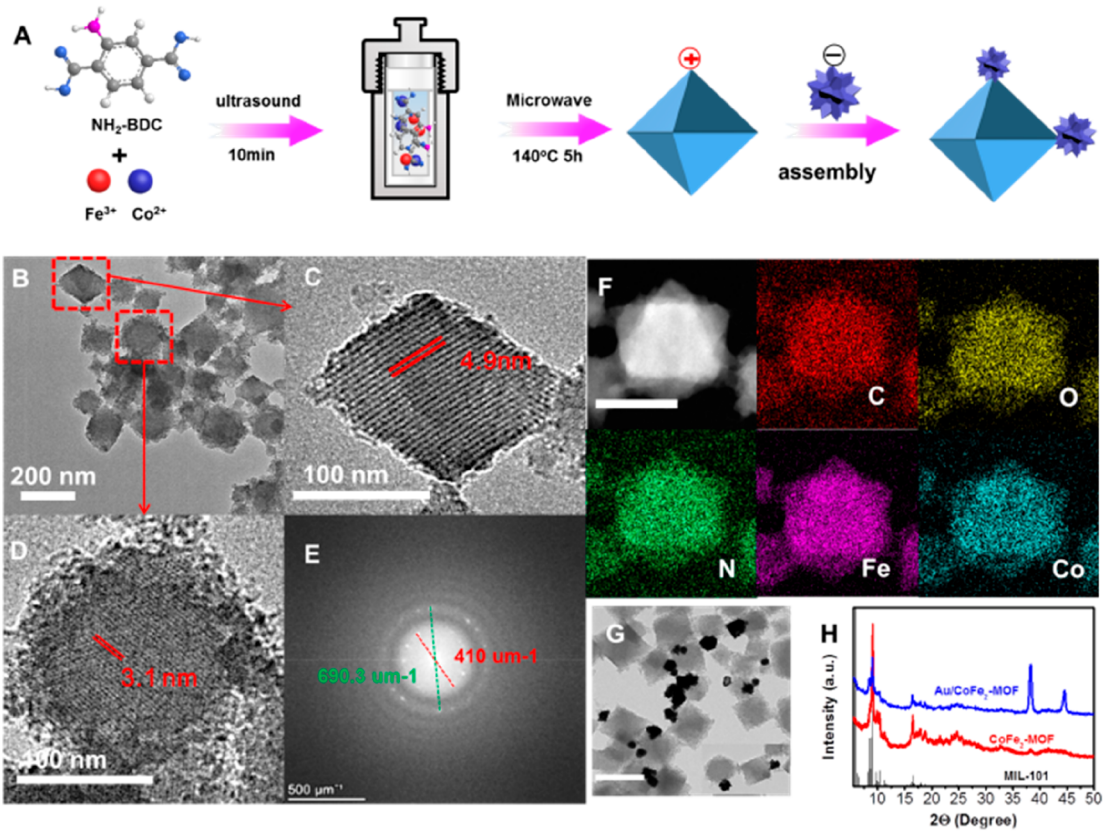

Figure 1. (A) Preparation process of Au/$CoFe_2$-MOFs. (B) TEM images of $CoFe_2$-MOFs. (C,D) HRTEM of $CoFe_2$-MOFs at different lattice planes. (E) FFT pattern of $CoFe_2$-MOF. (F) EDS images of a $CoFe_2$-MOF and the corresponding elemental mappings for C, N, O, Fe, and Co. (G) TEM image of Au/$CoFe_2$-MOFs. The scale bar is 200 nm. (H) X-ray diffraction pattern of $CoFe_2$-MOFs (black curve) and Au/$CoFe_2$-MOFs (red curve).

$CoFe_2$-MOFs (800 μL) for 1 h. Then, the NADH-MPBA-Au/$CoFe_2$-MOFs are collected by centrifugation (8000 rpm) and dispersed by PBS (1.0 mL, pH 7.4). NADH-MPBA-Au/$CoFe_2$-MOFs solutions (10.0 μL) at different concentrations are dropped onto aluminum foil for SERS measurements. For SERS studies, a 785 nm laser is used. and the collective time was 3 s for a one-time measurement. SERS signals from random spots on the substrates are recorded to investigate the reproducibility. For *in situ* SERS imaging, MPBA-Au/$CoFe_2$-MOFs solution (the final concentration was 10.0 μg/mL) is cultured with HeLa cells or L929 cells (1×10^5 cells/mL). Then, HeLa cells or L929 cells are cleaned by PBS three times. After that, HeLa cells or L929 cells are treated with glucose (10.0 mM) for 1 h or pyruvic acid (1.0 mM) for 30 min. The SERS imagings are recorded using the same conditions as above with extension of time.

RESULTS AND DISCUSSION

Characterization of Au/$CoFe_2$-MOFs. The synthesis of $CoFe_2$-MOFs is schematically described in Figure 1A. First, amine-1,4-dicarboxybenzene (NH_2−BDC), $FeCl_3 \cdot 6H_2O$, and $CoCl_2 \cdot 6H_2O$ are mixed in *N,N*-dimethylformamide (DMF) and dissolved by ultrasound. The mixture is then placed in a specific tube and the tube kept in a microwave oven.[21] The carboxyl groups of NH_2−BDC could be coordinated with Fe^{3+} and Co^{2+} at 140 °C to produce dark red $CoFe_2$-MOF powder (Figure S1 inset). As revealed by scanning transmission electron microscopy (SEM) and transmission electron microscope (TEM), $CoFe_2$-MOFs are octahedral with a relatively uniform size of ∼200 nm (Figure S1 and Figure 1B). The high-resolution TEM (HRTEM) image is employed to determine the crystal structures of $CoFe_2$-MOFs under the very low energy of an electron beam. As displayed in Figure 1C and D, the crystal planes belonging to [022] and [111] in $CoFe_2$-MOFs are collected.[24] The relevant fast Fourier transform (FFT) pattern of the $CoFe_2$-MOFs is shown in Figure 1E. Subsequently, energy dispersive X-ray spectroscopy (EDS) on TEM is used to determine the element composition and distribution. As shown in Figure 1F, the distribution of C, O, N, Co, and Fe elements is homogeneous on the entire $CoFe_2$-MOF particle, demonstrating that the proposed MOFs are bimetallic $CoFe_2$-MOFs rather than simply mixing Co-MOFs with Fe-MOFs. Inductively coupled plasma mass spectrometry (ICP-MS) quantified the proportion of Fe elements and Co elements in the $CoFe_2$-MOFs to be 3.27 and 1.48 wt %, respectively, which is almost equivalent to the feed ratio of $FeCl_3 \cdot 6H_2O$ and $CoCl_2 \cdot 6H_2O$ (2:1).

Gold nanostars (Au NSs) are synthesized using a typical surfactant-free method and modified with thiol caproic acid via Au−S bonds (Figure S2).[22,25] Au/$CoFe_2$-MOF hybrids are prepared by mixing negatively charged carboxyl modified Au NSs with positively charged $CoFe_2$-MOFs via electrostatic interactions (Figure 1A). The octahedral morphology of $CoFe_2$-MOFs is clearly observed by TEM (Figure 1G), and Au NSs (around 60−90 nm) are randomly distributed on the surface of MOFs. The zeta potentials of Au NSs, $CoFe_2$-MOFs, and Au/$CoFe_2$-MOFs are −32, +39, and +19 mV, respectively (Figure S3). Zeta potential changes further demonstrate that Au NSs are incorporated simply with $CoFe_2$-MOFs via electrostatic interactions.[25] The crystal structures of $CoFe_2$-MOFs and Au/$CoFe_2$-MOFs are further investigated by X-ray

https://doi.org/10.1021/acssensors.2c01175
ACS Sens. 2022, 7, 2671−2679

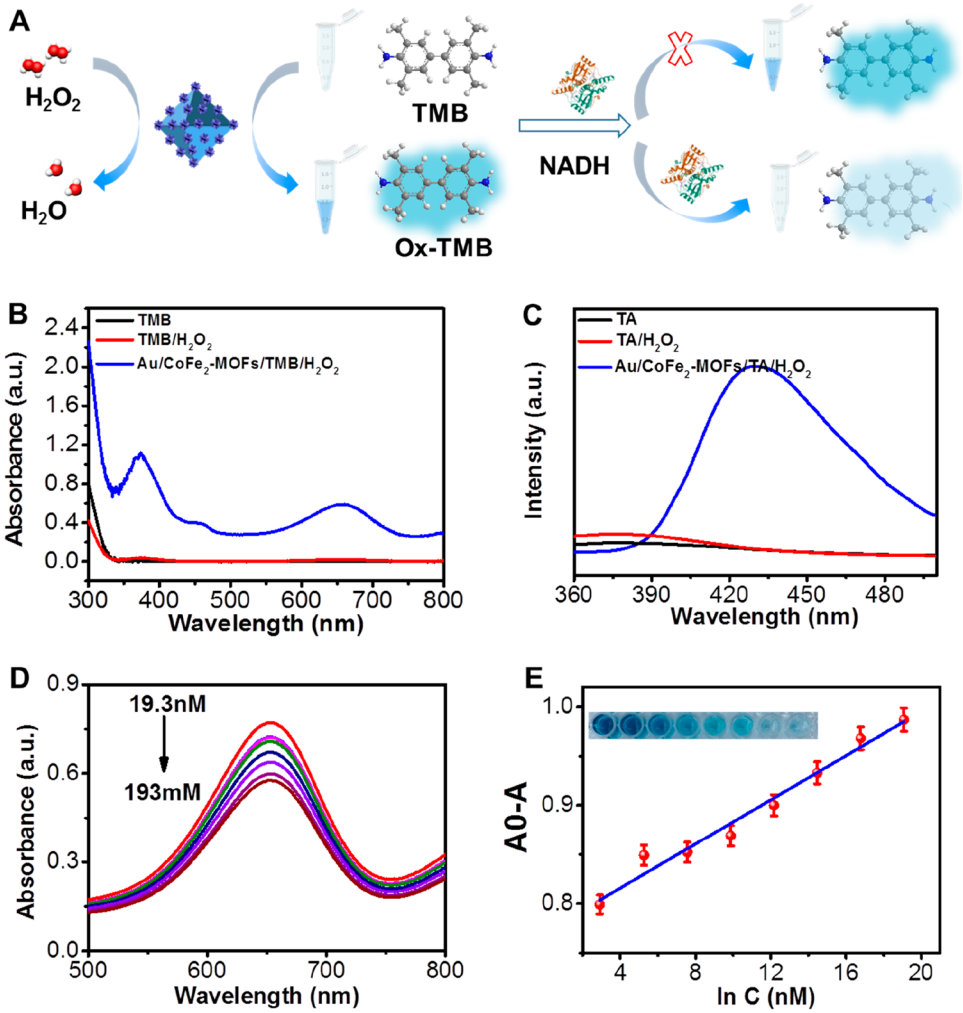

Figure 2. (A) Schematic illustration of the process for NADH detection by the colorimetric method. (B) UV−vis spectra of different groups in NAc-HAc buffer (pH 4.5, 20.0 mM) (black curve: TMB, red curve: H_2O_2/TMB, blue curve: Au/$CoFe_2$-MOFs/TMB/H_2O_2, respectively). The concentration of Au/$CoFe_2$-MOF was 0.1 mg/mL, that of H_2O_2 is 800.0 μM. and that of TMB is 1.0 mM in buffer solution. (C) Fluorescence spectra of different reaction systems (pH 4.5, 20.0 mM) after 10 min reaction. (Black curve: TA, red curve: TA/H_2O_2, blue curve: Au/$CoFe_2$-MOFs/TA/H_2O_2). (D) UV−vis spectra of ox-TMB after adding variable concentrations of NADH (the arrow: 19.3 nM to 193.0 mM). (E) Linear calibration plot of (A_0−A) versus the logarithm of NADH concentration. A_0: the absorbance of ox-TMB before adding NADH. A: the absorbance of ox-TMB after adding NADH. The inset is the color change after adding different concentrations of NADH. From left to right: the concentration of NADH increased. The error bars represent the standard deviation (n = 3 experiments).

diffraction patterns (XRD) (Figure 1H). The main peaks of $CoFe_2$-MOFs and Au/$CoFe_2$-MOFs at 7−30° are basically the same, ascribing to the NH_2-MIL-101(Fe) typical signals.[24,26] It also suggests that the crystal structure of $CoFe_2$-MOFs is not destroyed after decoration with Au NSs. In addition, the XRD spectrum of Au/$CoFe_2$-MOF powders displays two new characteristic peaks at 38.5° and 44.1°, consistent with Au [111] and Au [200].[25] Furthermore, Fourier transform infrared spectra (FT-IR) of $CoFe_2$-MOFs and Au/$CoFe_2$-MOFs are similar (Figure S4). On the basis of the related results, it could be assumed that the structure of $CoFe_2$-MOFs is not damaged after introducing Au NSs. Besides, X-ray photoelectron spectroscopy (XPS) analysis also provides more evidence to confirm the successful synthesis of the as-prepared Au/$CoFe_2$-MOFs shown in Figure S5.

NADH Detection by Colorimetric Method. As shown in Figure 2A, Au/$CoFe_2$-MOFs possess excellent peroxidase-like activity. In the presence of H_2O_2, Au/$CoFe_2$-MOFs can oxidize colorless 3,3′,5,5′-tetramethylbenzidine (TMB) to blue color oxidized TMB (ox-TMB) with a characteristic peak located at 652 nm,[27] which is absent from TMB and TMB/H_2O_2 (Figure 2B). Like natural horseradish peroxidase (HRP), the peroxidase-like activity of Au/$CoFe_2$-MOFs is concentration and pH dependent (Figure S6 and Figure S7). According to the Michaelis−Menten, the Michaelis−Menten constant (K_m) and the maximum reaction velocity (V_m) are calculated (Figure S8). When TMB and H_2O_2 serve as substrates, the V_m values of the Au/$CoFe_2$-MOFs at pH 4.5 are around 8.1×10^{-8} M s^{-1} and 6.4×10^{-8} M s^{-1}, respectively. Meanwhile, when TMB and H_2O_2 are introduced as substrates, the K_m values are about 0.162 mM and 0.092 μM, respectively. Au/$CoFe_2$-MOFs possess lower K_m and faster V_m compared to HRP,[28] suggesting the strongest affinity and higher reaction activities.

·OH radicals can cause the oxidation of TMB to blue ox-TMB, inducing the NADH detection by the colorimetric method; thus it is important to confirm whether ·OH radicals

https://doi.org/10.1021/acssensors.2c01175
ACS Sens. 2022, 7, 2671−2679

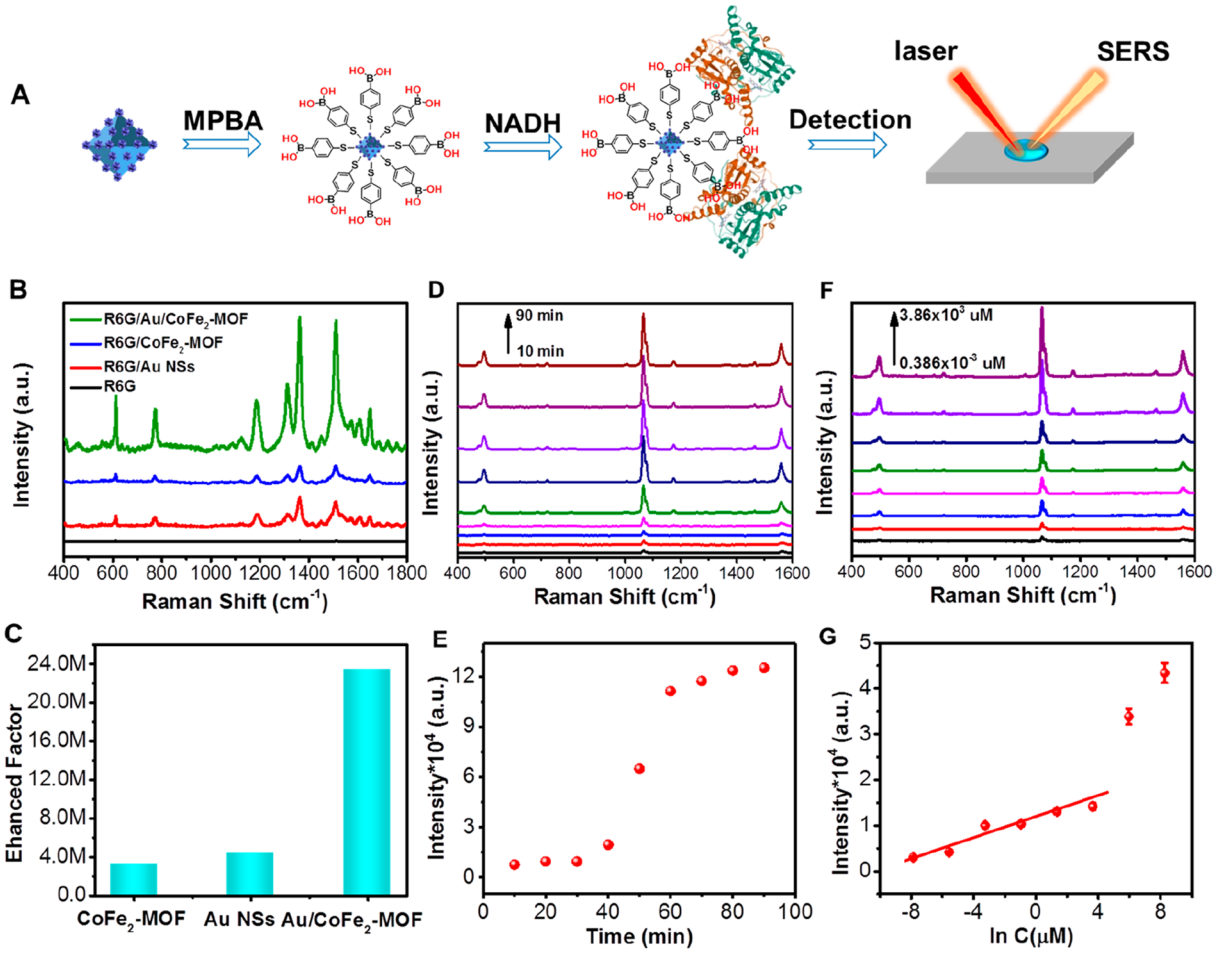

Figure 3. (A) Schematic illustration of the process for NADH detection. (B) SERS spectra of R6G molecules (10^{-1} M and 10^{-6} M) using aluminum, Au NSs, $CoFe_2$-MOFs, and Au/$CoFe_2$-MOFs as SERS substrates. (C) Corresponding enhanced factors (EFs). (D) Raman spectra of MPBA after adding NADH at different capture times. (E) SERS intensity at 1076 cm^{-1} versus capture time from (D). (F) Raman spectra of MPBA by variable concentrations of NADH (3.86×10^{-4} μM to 3.86×10^{3} μM). (G) Linear calibration plot between the increase of Raman intensity at 1076 cm^{-1} and the logarithm of NADH concentration. The error bars represent the standard deviation (n = 3 experiments).

are generated by this nanozyme. Terephthalic acid (TA) can be oxidized by ·OH radicals to produce a fluorescence product with a maximum emission wavelength of 447 nm.[27] Compared to other groups, there is an obvious peak at 447 nm for H_2O_2/Au/$CoFe_2$-MOFs system, indicating ·OH is generated due to the higher catalytic activity of Au/$CoFe_2$-MOFs (Figure 2C). To further demonstrate the generation of ·OH, the Raman spectra of ox-TMB are recorded during the catalytic process shown in Figure S9. The results suggested that the high peroxidase-mimic activity of Au/$CoFe_2$-MOFs can catalytically decompose H_2O_2 to produce ·OH, effectively oxidizing TMB to blue ox-TMB for further biosensor application based on the colorimetric method.

As a reductant, NADH suppresses the generation of blue ox-TMB catalyzed by Au/$CoFe_2$-MOFs (Figure 2A).[29] Thereby, a simple and naked-eye colorimetric detection for NADH is realized. As shown in Figure 2D, the absorbance at 652 nm decreased with increasing concentration of NADH. Consistently, visible color changes to colorless are observed as the concentration of NADH increases (Figure 2E inset). A good linear relationship between ${}_{\Delta}A$ (${}_{\Delta}A = A_0 - A$, A_0 is the absorbance at 652 nm before adding NADH shown in Figure S10) and the concentration of NADH from 19.3 nM to 193.0 mM has been found in Figure 2E. The error bars indicate the standard deviation. In our experiment (Figure 2E), each point represents the mean and standard deviation of the absorbance of ox-TMB from 3 parallel measurements after adding NADH with a defined concentration. The linearly fitted line is ${}_{\Delta}A = 0.01 \ln C + 0.77$ with an R value of 0.987. The limit of detection (LOD) is 2.7×10^{-9} M. Based on the above results, the colorimetric method shows an excellent capability for convenient and low-cost analysis of NADH without the need of complicated equipment. However, an acidic environment is required by the nanozymes-based colorimetric method, and this limits NADH dynamics study in living cells.

NADH Sensing by SERS. Au NSs can enhance the SERS signals by electromagnetic enhancement (EM),[16] and $CoFe_2$-MOFs have semiconducting-like properties, providing the chemical enhancement (CM) of Raman signals.[17] Due to the coexistence with the EM and CM, Au/$CoFe_2$-MOF hybrids are excellent candidates for the detection of NADH (Figure 3A). In this work, the SERS enhancement capacity on different substrates is determined by R6G molecule, and the Raman spectra of R6G (1.0×10^{-6} M) are recorded from MOFs, Au NSs, and Au/$CoFe_2$-MOFs under 785 nm laser irradiation, respectively (Figure 3B). Obviously, R6G bands are very weak

https://doi.org/10.1021/acssensors.2c01175
ACS Sens. 2022, 7, 2671−2679

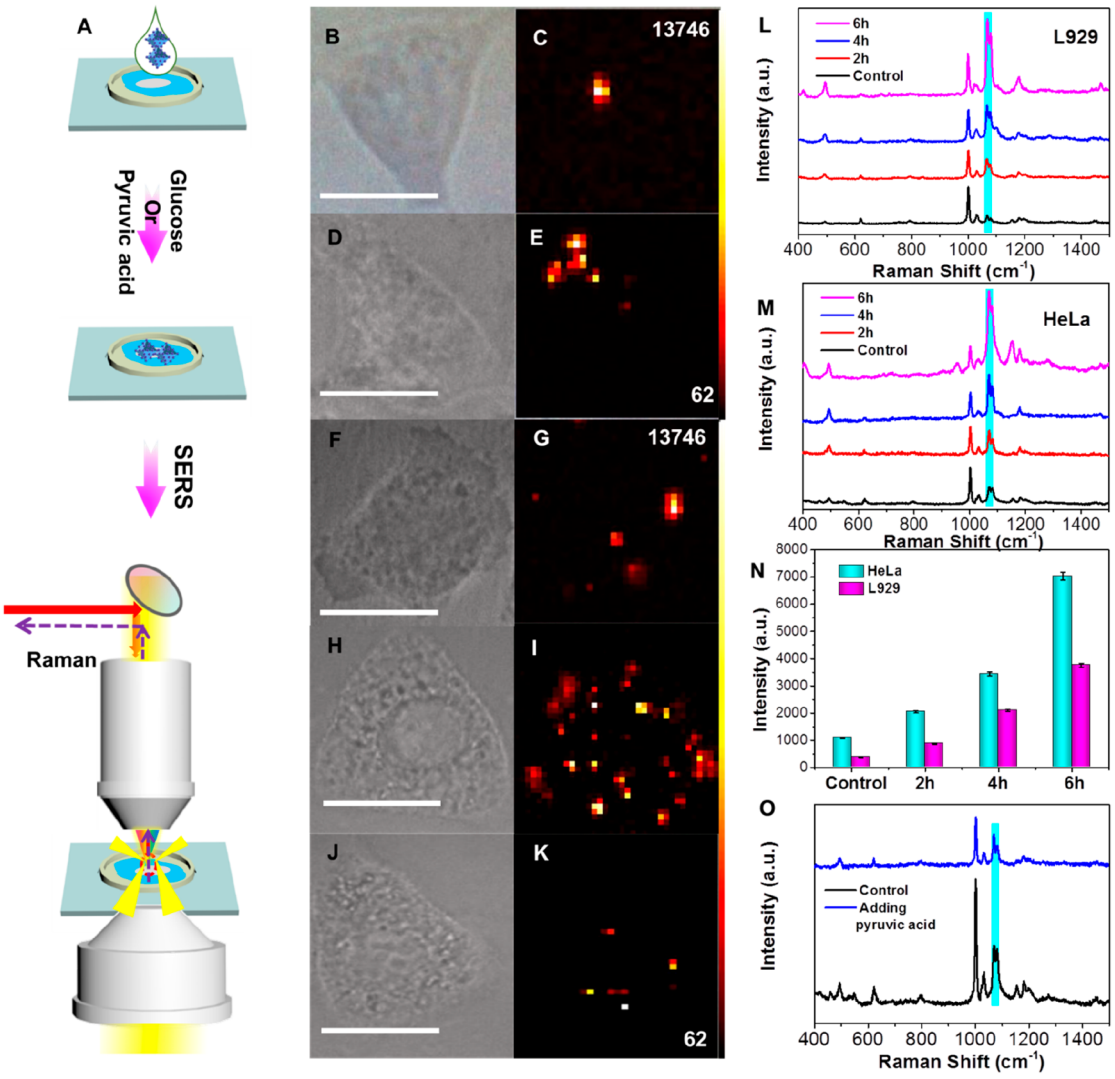

Figure 4. (A) Scheme of SERS imaging by MPBA-Au/$CoFe_2$-MOFs after treatment with different compounds. Bright-field image (B,D) and Raman image (C,E) of L929 cells before (B,C) and after (D,E) treatment with glucose (10.0 mM) at 1076 cm^{-1}. The scale bar is 10 μm. Bright-field image (F,H) and Raman image (G,I) of HeLa cells before (F,G) and after (H,I) treatment with glucose (10.0 mM) at 1076 cm^{-1}. The scale bar is 10 μm. Bright-field image (J) and Raman image (K) of HeLa cells after treatment with pyruvic acid (1.0 mM) at 1076 cm^{-1}. (L) Raman spectra of MPBA in L929 cells before and after treatment with 10.0 mM glucose within 6 h (n = 10 experiments). (M) Raman spectra of MPBA in HeLa cells before and after treatment with 10.0 mM glucose within 6h (n = 10 experiments). (N) Average Raman intensity at 1076 cm^{-1} in HeLa cells and L929 cells before and after treatment with 10.0 mM glucose at different times. The error bars represent the standard deviation (n = 10 experiments). (O) Raman spectra of MPBA in HeLa cells after treatment with pyruvic acid for 30 min.

on the aluminum even with higher concentration (1.0×10^{-1} M), whereas the peak intensities of R6G are noticeable on $CoFe_2$-MOFs and Au NSs substrates, attributing to the greater SERS enhancement via CM and EM, respectively. Interestingly, with the decoration of Au NSs on $CoFe_2$-MOFs, the highest peak intensity of R6G can be observed, attributed to the synergistic effect of the EM from Au NSs (called "hot-spot")[21] and the CM from the $CoFe_2$-MOFs. The average enhancement factors (EF) of Au NSs, $CoFe_2$-MOFs, and Au/$CoFe_2$-MOFs on the aluminum foil are calculated to be about 4.4×10^6, 3.2×10^6, and 2.3×10^7, respectively (Figure 3C).[23,30] Based on the above results, Au/$CoFe_2$-MOFs are employed for NADH detection on the basis of the SERS technique. Generally, target NADH is specifically captured by the boronic acid groups in 4-MPBA on Au/$CoFe_2$-MOFs.[9,31] After unwanted species are washed away, the captured NADH is then subjected to SERS detection.

To acquire more sensitive SERS signals, the optimized experiments for some parameters are conducted. In this work, the wavelength of the laser, the power of the laser, the concentration of MPBA, and the effect of the incubation time of NADH are the main factors influencing the sensitivity. As shown in Figure S11, the three strong Raman bands (1586 cm^{-1}, 1076 cm^{-1}, and 589 cm^{-1}) can be collected under three wavelengths of laser, attributed to C═C stretching, breathing vibration modes of the aromatic nucleus, and B−OH shear vibrations in the MPBA spectra, confirming that MPBA shows high SERS activity.[32] The following experiments are performed with a 785 nm laser in order to gain a higher Raman scattering intensity at 1076 cm^{-1} compared with a 532 or 633 nm laser, and the Raman intensity of MPBA at 1076 cm^{-1} is increased

https://doi.org/10.1021/acssensors.2c01175
ACS Sens. 2022, 7, 2671−2679

with increasing power of the 785 nm laser from 0.05% to 100% (Figure S12). The concentration of MPBA also has an influence on SERS signals (Figure S13). The characteristic Raman peaks at 1076 cm^{-1} gradually increase with increasing concentration of MPBA from 1.25 mM to 5.0 mM and then plateau after 5.0 mM, suggesting a saturation of MPBA modification.

The optimum hybridization time is investigated by mixing NADH solution (100.0 μL, 1.93 mM) with MPBA-Au/$CoFe_2$-MOFs solution (1.0 mL) and then incubated for different times (10, 20, 30, 40, 50, 60, 70, 80, and 90 min) at 4 °C. When the NADH solution incubates with MPBA-Au/$CoFe_2$-MOFs, the Raman intensity at 1076 cm^{-1} first increases and then remains constant after 60 min (Figure 3D). This phenomenon indicates that NADH molecules can specifically react to the boronic acid groups in MPBA, increasing the SERS intensity of MPBA under charge-transfer effects, and the action of orientation changes.[33] Then the Raman intensity reached a platform after 60 min, indicating complete hybridization. The intensity−time curve is shown in Figure 3E, which is in line with the result in Figure 3D.

The sensitivity is indispensable for evaluating the practicality of the established sensors. The concentration-dependent Raman measurements are evaluated on the Au/$CoFe_2$-MOF substrates. The Raman intensity at 1076 cm^{-1} increases gradually with the increase of NADH concentration from 3.86 × 10^{-4} μM to 3.86 × 10^{3} μM (Figure 3F). The plot of intensity (I) versus the logarithm concentration (3.86 × 10^{-4} μM to 3.86 μM) of NADH shows that the relative SERS intensity linearly increases depending on the concentration (Figure 3G). The linearly fitted line is I = 1029 ln C + 11314 with an R^2 value of 0.979. Notably, as the concentration of NADH rises to 38.6 μM, the Raman intensity shows a sharp increase. The limit of detection (LOD) can be achieved to 2.8 × 10^{-11} M (the calculation process is shown in Supporting Information), which is much lower than that of the most reported methods depicted in Table S1. To evaluate the reproducibility of the present sensor, the reproducibility is first determined by repeatedly detecting NADH molecules (1.93 mM) on Au/$CoFe_2$-MOFs substrate at different spots on the same batch (Figure S14), and the SERS intensities at 1076 cm^{-1} are averaged with five measurements. This method shows excellent reproducibility with a quite low value of relative standard deviation (RSD) of about 5.0%. Similarly, the batch-to-batch reproducibility is also acceptable with the RSD of 7.8%. To evaluate the specificity of the proposed biosensor for NADH detection, several relevant interference species were selected for testing, including albumin from bovine serum (BSA), glucose (Glu), and glutathione (GSH). These molecules even at a much higher concentration than NADH (100 vs 2 mM) did not cause significant interference with the detection BSA; Glu and GSH gave negligible SERS signal, whereas the SERS intensity increased rapidly after adding NADH, indicating that SERS can specifically detect NADH (Figure S15). The results demonstrate that the proposed sensor exhibits excellent specificity toward NADH.

NADH Dynamics in Living Cells. Inspired by the excellent performance of this NADH probe *in vitro*, the application of the proposed sensor for monitoring NADH dynamics is evaluated in live normal cells and human cancer cells. The cytotoxicity of Au/$CoFe_2$-MOFs is first assessed before the bioimaging analysis. Two different cell lines (fibroblast cells (L929) and human cervical cancer cells (HeLa)) are used to carry out the toxicity assay. Obviously, the Au/$CoFe_2$-MOFs showed negligible toxicity inside living cells even the concentration is as high as 200 μg/mL (Figure S16). Therefore, Au/$CoFe_2$-MOFs are suitable candidates for bioimaging analysis of living cells. Besides, added materials further improved the negligible effect on the production of NADH in cells. Specifically, two cell groups at the same concentration (5 × 10^5 cells/mL) with or without materials were cultured; the NADH was then extracted and quantified by the colorimetric method as described in the Experimental Section (Figure S17). Obviously, the material had a slight effect on the production of NADH, which was conducive to the *in situ* study of intracellular NADH concentration and distribution. Owing to the limitation of the *in situ* colorimetric method, SERS technique is used to investigate the metabolic NADH dynamics in living cells (Figure 4A). It is reported that intracellular NADH levels show an enhanced response during glucose metabolism.[4] To demonstrate the capability of MPBA-Au/$CoFe_2$-MOFs for detecting intracellular NADH, living cells are treated with glucose (10 mM). The SERS images of cells are collected using Raman Spectroscopy (Figure 4B−K). As expected, when treated with 10 mM glucose, MPBA-Au/$CoFe_2$-MOFs incubated cells show a stronger Raman response at 1076 cm^{-1} from the SERS mapping (Figure 4E and I) than in the absence of glucose (Figure 4C and G). Meanwhile, the Raman spectra of MPBA are measured in the living cells, upon pretreatment with glucose. Both L929 cells (Figure 4L) and HeLa cells (Figure 4M) exhibit an increase in the intensity at 1076 cm^{-1}, which directly correlate with the increase in intracellular NADH levels. In the time-dependent study, the amount of NADH molecules increases within time from 2 to 6 h in either HeLa cells or L929 cells. The reason for this is that the relevant fluctuations of glucose levels have a significant effect on the NADH level, thereby resulting in a gradually increased NADH during glucose metabolism.[34] Interestingly, the Raman intensity at 1076 cm^{-1} is larger in cancer cells (HeLa cells, Figure 4N) than that in normal cells (L929 cells, Figure 4N). The phenomenon is explained as followings:[35,36] (1) The rapid proliferation of cancer cells demands more energy, giving rise to higher glucose consumption when compared to normal cells, which can cause higher NADH generation in cancer cells. (2) When glucose concentrations exceed physiological levels, altered metabolism can result from the high levels of glucose uptake and increased conversion of glucose via the glycolytic pathway (Warburg effect proposed by Nobel laureate Otto Warburg).[36] In addition, overproduced pyruvic acid converts into lactic acid in the glycolysis pathway in cancer cells, which would accelerate the consumption of NADH.[10] Therefore, MPBA-Au/$CoFe_2$-MOFs as a SERS probe are used to determine the NADH level after adding pyruvic acid. As shown in Figure 4J,K, the Raman signal at 1076 cm^{-1} from the SERS mapping is weaker than that in the absence of pyruvic acid. The Raman intensity at 1076 cm^{-1} also decreases, indicating the decrease in intracellular NADH levels after treatment with pyruvic acid (Figure 4O). These results demonstrate that the probe is a quite promising SERS tool for the determination of endogenous NADH and cellular imaging, which is consistent with previously reported work.[9] To verify the accuracy of the Raman results, NADH is extracted from cells to quantify via the colorimetric method as shown in Figure S18. It could be seen that the absorbance of ox-TMB at 652 nm decreases in cells after being treated with glucose, indicating more NADH generation after the addition

https://doi.org/10.1021/acssensors.2c01175
ACS Sens. 2022, 7, 2671−2679

of glucose. In contrast, the absorbance at 652 nm increases after being treated with pyruvic acid due to reduced NADH production. In addition, the absorbance of ox-TMB at 652 nm is lower in HeLa cells than that in L929 cells, suggesting the higher content of NADH in cancer cells. The results are in line with the result of *in situ* SERS measurement. Therefore, the proposed dual-mode biosensor is not only capable of the facile and fast naked-eye detection of NADH but also a *in situ* supersensitive SERS probe for monitoring NADH dynamics in living cells.

CONCLUSION

In summary, a new colorimetric and SERS dual-mode sensor based on Au/$CoFe_2$-MOFs is developed, which shows significant Raman enhancement and colorimetric response toward NADH. Based on the colorimetric mode, NADH can be detected with the naked eye in a linear range of 1.93×10^{-8} to 1.93×10^{-1} M with the LOD of 2.7×10^{-9} M. Such a sensor also shows a high sensitivity with a wide linear range of 3.86×10^{-10} M to 3.86×10^{-3} M based on SERS detection with the LOD of 2.8×10^{-11} M. Furthermore, the intracellular distribution of NADH and its dynamics during glycometabolism are revealed. This sensor represents a unique tool to reveal dynamic cellular processes involving NADH and identify the difference between cancerous cells and normal cells.

ASSOCIATED CONTENT

Supporting Information

The Supporting Information is available free of charge at https://pubs.acs.org/doi/10.1021/acssensors.2c01175.

General information, experimental section, additional characterized data, steady-state kinetic assay, the optimized experiments for some parameters, UV−vis spectra data under different conditions, and cell viability (PDF)

AUTHOR INFORMATION

Corresponding Authors

Lingjie Meng − *School of Chemistry, Xi'an Key Laboratory of Sustainable Energy Material Chemistry, Xi'an Jiaotong University, Xi'an 710049, China; Talent Highland, The First Affiliated Hospital, Xi'an Jiaotong University, Xi'an 710061, China; Instrumental Analysis Center of Xi'an Jiaotong University, Xi'an 710049, China;* orcid.org/0000-0003-0428-9780; Email: menglingjie@mail.xjtu.edu.cn

Peng Chen − *School of Chemistry, Chemical Engineering and Biotechnology, Institute for Digital Molecular Analytics and Science, Nanyang Technological University, 637457, Singapore;* orcid.org/0000-0003-3730-1846; Email: chenpeng@ntu.edu.sg

Authors

Xiaoping Zhao − *School of Chemistry, Xi'an Key Laboratory of Sustainable Energy Material Chemistry, Xi'an Jiaotong University, Xi'an 710049, China*

Ruoxin Niu − *School of Chemistry, Xi'an Key Laboratory of Sustainable Energy Material Chemistry, Xi'an Jiaotong University, Xi'an 710049, China*

Shu Fan − *School of Chemistry, Xi'an Key Laboratory of Sustainable Energy Material Chemistry, Xi'an Jiaotong University, Xi'an 710049, China*

Xunan Jing − *Talent Highland, The First Affiliated Hospital, Xi'an Jiaotong University, Xi'an 710061, China*

Rui Gao − *School of Chemistry, Xi'an Key Laboratory of Sustainable Energy Material Chemistry, Xi'an Jiaotong University, Xi'an 710049, China*

Hongbo Yang − *School of Chemistry, Xi'an Key Laboratory of Sustainable Energy Material Chemistry, Xi'an Jiaotong University, Xi'an 710049, China*

Heng Wang − *School of Chemistry, Xi'an Key Laboratory of Sustainable Energy Material Chemistry, Xi'an Jiaotong University, Xi'an 710049, China*

Daquan Wang − *School of Chemistry, Xi'an Key Laboratory of Sustainable Energy Material Chemistry, Xi'an Jiaotong University, Xi'an 710049, China*

Zhiwei Yang − *School of Physics, MOE Key Laboratory for Nonequilibrium Synthesis and Modulation of Condensed Matter, Xi'an Jiaotong University, Xi'an 710049, China;* orcid.org/0000-0001-6158-8803

Yunchuan Xie − *School of Chemistry, Xi'an Key Laboratory of Sustainable Energy Material Chemistry, Xi'an Jiaotong University, Xi'an 710049, China;* orcid.org/0000-0003-0202-384X

Junjun She − *Talent Highland, The First Affiliated Hospital, Xi'an Jiaotong University, Xi'an 710061, China*

Complete contact information is available at: https://pubs.acs.org/10.1021/acssensors.2c01175

Author Contributions

The manuscript was written through the contributions of all authors. All authors have given approval to the final version of the manuscript.

Notes

The authors declare no competing financial interest.

ACKNOWLEDGMENTS

This work was supported by the National Natural Science Foundation of China (21674085), National Postdoctoral Program for Innovative Talent (BX20190277), the Natural Science Basic Research Plan in Shaanxi Province of China (2020JZ-01), the China Postdoctoral Science Foundation (2020M673387, 2021M702557), the Key Laboratory Construction Program of Xi'an Municipal Bureau of Science and Technology (201805056ZD7CG40), the youth talent support program of Xi'an Jiaotong University (HX6J016) and Singapore Ministry of Education under its Academic Research Fund (AcRF) Tier-1 grants (RG110/20 and RT02/20) and AcRF Tier-2 grant (MOE2019-T2-2-004). We would like to thank Dr Chao Li, Dr Chang Huang, Dr Huimin Tong, Dr Hang Guo, Miss Ying Hao, Miss Jiamei Liu, and Mr. Jiaxiang Sun at the Instrumental Analysis Center of Xi'an Jiaotong University for their assistance with characterizations.

REFERENCES

(1) Gómez-Virgilio, L.; Luarte, A.; Ponce, D. P.; Bruna, B. A.; Behrens, M. I. Analyzing Olfactory Neuron Precursors Non-Invasively Isolated through NADH FLIM as A Potential Tool to Study Oxidative Stress In Alzheimer's Disease. *Int. J. Mol. Sci.* **2021**, *22*, 6311.

(2) Berthiaume, J. M.; Kurdys, J. G.; Muntean, D. M.; Rosca, M. G. Mitochondrial NAD^+/NADH Redox State And Diabetic Cardiomyopathy. *Antioxid. Redox Signal.* **2019**, *30*, 375−398.

(3) Jafri, M. S.; Dudycha, S. J.; O'Rourke, B. Cardiac Energy Metabolism: Models of Cellular Respiration. *Annu. Rev. Biomed. Eng.* **2001**, *3*, 57−81.
(4) Chiarugi, A.; Dölle, C.; Felici, R.; Ziegler, M. The NAD Metabolome -A Key Determinant Of Cancer Cell Biology. *Nat. Rev. Cancer.* **2012**, *12*, 741−752.
(5) Cui, Y. H.; Shi, Q. S.; Zhang, D. D.; Wang, L. L.; Feng, J.; Chen, Y. W.; Xie, X. B. Detoxification Of Ionic Liquids Using Glutathione, Cysteine, And NADH: Toxicity Evaluation By Tetrahymena Pyriformis. *Environ. Pollut.* **2021**, *276*, 116725.
(6) Li, J.; Sun, Q.; Mao, Y.; Bai, Z.; Ning, X.; Zheng, J. Sensitive And Low-Potential Detection Of NADH Based On Boronic Acid Functionalized Multi-Walled Carbon Nanotubes Coupling With An Electrocatalysis. *J. Electroanal. Chem.* **2017**, *794*, 1−7.
(7) Akhtar, M. H.; Mir, T.; Gurudatt, N. G.; Chung, S.; Shim, Y. B. Sensitive NADH Detection In A Tumorigenic Cell Line Using A Nano-Biosensor Based On The Organic Complex Formation. *Biosens. Bioelectron.* **2016**, *85*, 488−495.
(8) Podder, A.; Thirumalaivasan, N.; Chao, Y. K.; Kukutla, P.; Wu, S. P.; Bhuniya, S. Two-Photon Active Fluorescent Indicator for Detecting NADH Dynamics In Live Cells And Tumor Tissue. *Sensor. Actuat. B-Chem.* **2020**, *324*, 128637.
(9) Wang, L.; Zhang, J.; Kim, B.; Peng, J.; Berry, S. N.; Ni, Y.; Su, D.; Lee, J.; Yuan, L.; Chang, Y. T. Boronic Acid: A Bio-Inspired Strategy to Increase the Sensitivity and Selectivity of Fluorescent NADH Probe. *J. Am. Chem. Soc.* **2016**, *138*, 10394−10397.
(10) Podder, A.; Murali, V. P.; Deepika, S.; Dhamija, A.; Biswas, S.; Maiti, K. K.; Bhuniya, S. NADH-Activated Dual-Channel Fluorescent Probes for Multicolor Labeling of Live Cells and Tumor Mimic Spheroids. *Anal. Chem.* **2020**, *92*, 12356−12362.
(11) Yamada, K.; Hara, N.; Shibata, T.; Osago, H.; Tsuchiya, M. The Simultaneous Measurement Of Nicotinamide Adenine Dinucleotide And Related Compounds By Liquid Chromatography/Electrospray Ionization Tandem Mass Spectrometry. *Anal. Biochem.* **2006**, *352*, 282−285.
(12) Li, J. F.; Huang, Y. F.; Ding, Y.; Yang, Z. L.; Li, S. B.; Zhou, X. S.; Fan, F. R.; Zhang, W.; Zhou, Z. Y.; Wu, D. Y.; Ren, B.; Wang, Z. L.; Tian, Z. Q. Shell Isolated Nanoparticle Enhanced Raman Spectroscopy. *Nature* **2010**, *464*, 392−395.
(13) Masson, J. F. Surface Plasmon Resonance Clinical Biosensors for Medical Diagnostics. *ACS Sens.* **2017**, *2*, 16−30.
(14) Lussier, F.; Brulé, T.; Vishwakarma, M.; Das, T.; Spatz, J. P.; Masson, J. F. Dynamic-SERS Optophysiology: A Nanosensor for Monitoring Cell Secretion Events. *Nano Lett.* **2016**, *16*, 3866−3871.
(15) Zhao, X.; Campbell, S.; Wallace, G. Q.; Claing, A.; Bazuin, C. G.; Masson, J. F. Branched Au Nanoparticles on Nanofibers for Surface-Enhanced Raman Scattering Sensing of Intracellular pH and Extracellular pH Gradients. *ACS Sens.* **2020**, *5*, 2155−2167.
(16) Langer, J.; de Aberasturi, D. J.; Aizpurua, J.; Alvarez-Puebla, R. A.; Jeremy, J.; Baumberg, B. A.; Steven, E. J.; Bell, G. C. B.; Alexandre, G.; Brolo, A. B.; Dana Cialla-May, J. C.; Laura Fabris, V. D.; Javier García, F.; de Abajo, K. F.; Duncan Graham, R. G.; Christy, L.; Haynes, A. J. H.; et al. Present and Future of Surface-Enhanced Raman Scattering. *ACS Nano* **2020**, *14* (1), 28−117.
(17) Pettine, J.; Choo, P.; Medeghini, F.; Odom, T. W.; Nesbitt, D. J. Plasmonic Nanostar Photocathodes For Optically Controlled Directional Currents. *Nat. Commun.* **2020**, *11*, 1367.
(18) Shao, Q.; Zhang, D.; Wang, C.; Tang, Z.; Zou, M.; Yang, X.; Gong, H.; Yu, Z.; Jin, S.; Liang, P. Ag@MIL-101(Cr) Film Substrate with High SERS Enhancement Effect and Uniformity. *J. Phys. Chem. C* **2021**, *125*, 7297−7304.
(19) Sun, H.; Cong, S.; Zheng, Z.; Wang, Z.; Chen, Z.; Zhao, Z. Metal-Organic Frameworks as Surface Enhanced Raman Scattering Substrates with High Tailorability. *J. Am. Chem. Soc.* **2019**, *141*, 870−878.
(20) Huang, X.; Zhang, S.; Tang, Y.; Zhang, X.; Bai, Y.; Pang, H. Advances In Metal-Organic Framework-Based Nanozymes And Their Applications. *Coordin. Chem. Rev.* **2021**, *449*, 214216.
(21) Li, X.; Guo, W.; Liu, Z.; Wang, R.; Liu, H. Quinone-Modified NH_2-MIL-101(Fe) Composite As A Redox Mediatorfor Improved Degradation Of Bisphenol A. *J. Hazard. Mater.* **2017**, *324*, 665−672.
(22) Wang, C.; Zhao, X. P.; Xu, Q. Y.; Nie, X. G.; Younis, M. R.; Liu, W. Y.; Xia, X. H. Importance of Hot Spots in Gold Nanostructures on Direct Plasmon-Enhanced Electrochemistry. *ACS Appl. Nano Mater.* **2018**, *1*, 5805−5811.
(23) Li, Q.; Gong, S.; Zhang, H.; Huang, F.; Zhang, L.; Li, S. Tailored Necklace-Like Ag@ZIF-8 Core/Shell Heterostructure Nanowires For High-Performance Plasmonic SERS Detection. *Chem. Eng. J.* **2019**, *371*, 26−33.
(24) Zhao, X.; Zhang, N.; Yang, T.; Liu, D.; Jing, X.; Wang, D.; Yang, Z.; Xie, Y.; Meng, L. Bimetallic Metal-Organic Frameworks: Enhanced Peroxidase-like Activities for the Self-Activated Cascade Reaction. *ACS Appl. Mater. Interfaces* **2021**, *13*, 36106−36116.
(25) Wang, S. S.; Jiao, L.; Qian, Y.; Hu, W. C.; Xu, G. Y.; Wang, C.; Jiang, H. L. Boosting Electrocatalytic Hydrogen Evolution over Metal-Organic Frameworks by Plasmon-Induced Hot-Electron Injection. *Angew. Chem., Int. Ed.* **2019**, *58*, 10713−10717.
(26) Fu, J.; Wang, L.; Chen, Y.; Yan, D.; Ou, H. Enhancement Of Aqueous Stability Of NH_2-MIL-101(Fe) By Hydrophobic Grafting Post-Synthetic Modification. *Environ. Sci. Pollut. Res.* **2021**, *28*, 68560−68571.
(27) Xu, B.; Wang, H.; Wang, W.; Gao, L.; Li, S.; Pan, X.; Wang, H.; Yang, H.; Meng, X.; Wu, Q.; Zheng, L.; Chen, S.; Shi, X.; Fan, K.; Yan, X.; Liu, H. A Single-Atom Nanozyme for Wound Disinfection Applications. *Angew. Chem., Int. Ed.* **2019**, *58*, 4911−4916.
(28) Gao, L.; Zhuang, J.; Nie, L.; Zhang, J.; Zhang, Y.; Gu, N.; Wang, T.; Feng, J.; Yang, D.; Perrett, S.; Yan, X. Intrinsic Peroxidase-like Activity of Ferromagnetic Nanoparticles. *Nat. Nanotechnol.* **2007**, *2*, 577−583.
(29) Sandor, R.; Slanina, J.; Midlik, A.; Sebrlova, K.; Novotna, L.; Carnecka, M.; Slaninova, I.; Taborsky, P.; Taborska, E.; Pes, O. Sanguinarine is Reduced by NADH Through a Covalent Adduct. *Phytochemistry* **2018**, *145*, 77−84.
(30) Wang, Q.; Xu, Z.; Zhao, Y.; Zhangsun, H.; Bu, T.; Zhang, C.; Wang, X.; Wang, L. Bio-Inspired Self-Cleaning Carbon Cloth Based On Flower-Like Ag Nanoparticles And Leaf-Like MOF: A High-Performance And Reusable Substrate For SERS Detection Of Azo Dyes In Soft Drinks. *Sensor. Actuat. B-Chem.* **2021**, *329*, 129080.
(31) Sun, F.; Bai, T.; Zhang, L.; Ella-Menye, J. R.; Liu, S.; Nowinski, A. K.; Jiang, S.; Yu, Q. Sensitive and Fast Detection Of Fructose in Complex Media via Symmetry Breaking and Signal Amplification Using Surface-Enhanced Raman Spectroscopy. *Anal. Chem.* **2014**, *86*, 2387−2394.
(32) Zhao, Q.; Zhang, H.; Fu, H.; Wei, Y.; Cai, W. Raman Reporter-Assisted Au Nanorod Arrays SERS Nanoprobe for Ultrasensitive Detection of Mercuric Ion (Hg^{2+}) with Superior Anti-Interference Performances. *J. Hazard. Mater.* **2020**, *398*, 122890.
(33) Gao, D.; Yang, X.; Luo, M.; Teng, P.; Zhang, H.; Liu, Z.; Gao, S.; Li, Z.; Wen, X.; Yuan, L.; Li, K.; Bowkett, M.; Copner, N. Surface-Enhanced Raman Spectroscopy Detection of Cerebrospinal Fluid Glucose Based on the Optofluidic in-Fiber-Integrated Composites of Graphene Oxide, Silver Nanoparticles, and 4-Mercaptophenylboronic Acid. *ACS Appl. Nano Mater.* **2021**, *4*, 10784−10790.
(34) Zhao, Y.; Wei, K.; Kong, F.; Gao, X.; Xu, K.; Tang, B. Dicyanoisophorone-Based Near-Infrared-Emission Fluorescent Probe for Detecting NAD(P)H in Living Cells and in Vivo. *Anal. Chem.* **2019**, *91*, 1368−1374.
(35) Madhurantakam, S.; Babu, K. J.; Balaguru Rayappan, J. B.; MaheswariKrishnan, U. Fabrication of Mediator-free Hybrid Nano-interfaced Electrochemical Biosensor for Monitoring Cancer Cell Proliferation. *Biosens. Bioelectron.* **2017**, *87*, 832−841.
(36) Asgari, Y.; Zabihinpour, Z.; Salehzadeh-Yazdi, A.; Schreiber, F.; Masoudi-Nejad, A. Alterations in cancer cell metabolism: The Warburg effect and metabolic adaptation. *Genomics* **2015**, *105*, 275−281.

https://doi.org/10.1021/acssensors.2c01175
ACS Sens. 2022, 7, 2671−2679